JOURNAL OF Materials CHEMISTRY

Lamellar phases and microemulsions in model ternary blends containing amphiphilic block copolymers†

Laurence Corvazier, Loic Messé, Corinne L.O. Salou, Ronald N. Young, J. Patrick A. Fairclough and Anthony J. Ryan*

The Polymer Centre, Department of Chemistry, University of Sheffield, Sheffield, UK S3 7HF

Received 12th June 2001, Accepted 12th July 2001
First published as an Advance Article on the web 26th September 2001

The order–disorder transition (ODT), microdomain structures and the phase diagram for ternary blends of low molecular weight PS, PI and PS–PI have been determined by a combination of X-ray scattering and transmission electron microscopy. The distribution of the homopolymer within the layers of a related PS/PB/PS–PB system has also been determined by a combination of X-ray and neutron reflectivity.

A series of nearly symmetric, ternary blends of polystyrene (PS), polyisoprene (PI) and polystyrene-*block*-polyisoprene (PS–PI) have been studied by small angle X-ray scattering, static light scattering and transmission electron microscopy. The molecular weight of the homopolymers and block copolymer were in the ratio $N_H/N_{BCP}=0.19$, which gave a block copolymer ODT and a homopolymer blend T_C that were similar ($T_C/T_{ODT}\approx 1.1$). The block copolymer and its blends showed a weakly first-order transition from a lamellar phase to a fluctuating disordered phase in the volume fraction range $\Phi_H \leqslant 0.77$. A bicontinuous microemulsion was found between $\Phi_H=0.79$ and $\Phi_H=0.93$, and for $\Phi_H \geqslant 0.93$ macrophase separation was observed. In a similar PS, polybutadiene (PB) and polystyrene-*block*-polybutadiene (PS–PB) system the distribution of the homopolymer diluent was studied by X-ray and neutron reflectivity with deuterium labelled PS. The initial microstructure formed on spin coating had a dry-brush structure with the homopolymer concentrated in the centre of the domains and on subsequent annealing a wet-brush morphology was observed with the homopolymers uniformly distributed.

Introduction

Self-assembly of amphiphilic molecules provides one of the fundamental structure directing processes for building hierarchical structures in nature.[1] The universality of pattern formation across lipid membranes, lyotropic and thermotropic liquid crystals, and block copolymers, all soft-structures that are closely related to biological materials, is striking. Classical structures of lamellae, hexagonally ordered cylinders and cubic arrays of spheres are well established.[2] Complex cubic structures, such as the bicontinuous double diamond (*Pn*3*m*) and gyroid (*Ia*3*d*) have been found in lyotropic liquid crystals[3] and in block copolymer melts[2,4–7] and solutions[2,8,9] as well as in naturally occurring lipids.[10,11] For symmetric block copolymers lamellar morphologies are observed which comprise layers of molecules and could be classified as thermotropic smectic liquid crystals; cylinder morphologies are also formed, at certain compositions, that could be classified as thermotropic columnar liquid crystals. The cross-over between block copolymer behaviour (in terms of molecular weight scaling) and smectic liquid crystal behaviour has been tested and polymeric properties are found at quite modest molecular weights.[12] Block copolymers are amphiphilic and in the presence of one or more solvents will form lyotropic liquid crystals with the familiar lamellar, hexagonal, bicontinuous and cubic morphologies associated with low molecular weight surfactants.[13]

Theoretical aspects of microphase separation in block copolymers have been reviewed,[2,4,14] and relevant references can be found therein. Major contributions have come from self-consistent mean-field (SCF) theories[14–17] exemplified by the most recent predictions by Matsen and coworkers.[14] Considering an AB block copolymer comprising $N=N_A+N_B$ chain units, each occupying the same volume (v) and having the same statistical length (b), theory predicts equilibrium phase behaviour dependent only on the product χN and the composition defined by the mole fraction of A chain units, $x_A=N_A/N$. For this special case, parameter b is uniquely determined by the radius of gyration of the copolymer,

$$R_g^2 = Nb^2/6 \quad (1)$$

and parameter χ by the non-combinatorial Gibbs energy of mixing.

$$\Delta_{mix}G_{nc} = kT\chi N_A x_B = kT(\chi N)x_A x_B \quad (2)$$

For the copolymers of interest here, the unlike segments mix endothermically, and the temperature dependence of χ will be given approximately by

$$\chi = \alpha + \beta/T \quad (3)$$

where α and β are constants dependent on molecular composition. Microphase separation is favoured by lowering the temperature.

The main features of microphase separation in such a block copolymer system are clear. At low values of χN the block copolymer comprises a single disordered phase in which the chains have unperturbed dimensions.[14,17] Connectivity leads to a characteristic correlation length scaling as the radius of gyration, *i.e.* as $N^{1/2}$. Microphase separation is predicted at $\chi N\approx 10.5$ (the weak segregation limit, WSL). Free-energy minimisation results in the formation of ordered structures which are dependent on the composition.[2,14,15,17] The surface curvature and domain size is effectively set by a subtle balance between the surface area per chain, surface curvature and chain

†Basis of a presentation given at Materials Discussion No. 4, 11–14 September 2001, Grasmere, UK.

 DOI: 10.1039/b105165m

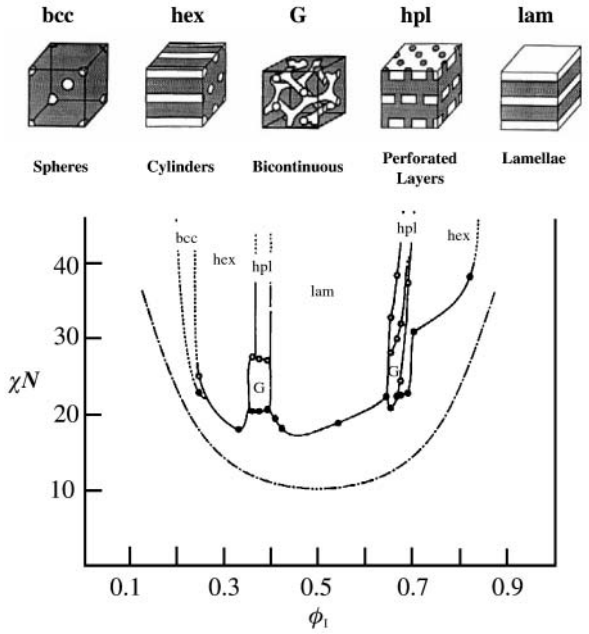

Fig. 1 Experimental phase diagram for low molar mass PS–PI block copolymers, the closed circles represent order–disorder transitions (ODT) and the open circles order–order-transitions (OOT); the solid curve is a guide to the eye. The ODT and OOTs were determined by rheology and the structures by a combination of TEM, SANS and SAXS.[6,16] The dotted curve is the mean field phase boundary after Liebler.[17]

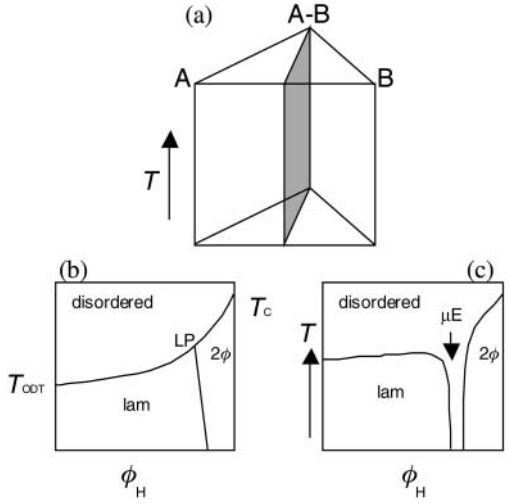

Fig. 2 (a) The phase prism for a three-component system, (b) a schematic of the theoretically predicted isopleth at equal volmes of A and B with the order–disorder temperature of the neat block copolymer, T_{ODT}, and the critical point of the homopolymer blend, T_C, marked, (c) a schematic of the experimentally observed isopleth for an A/B/A–B homopolymer block copolymer mixture. lam = lamellar phase, μE = microemulsion channel, 2ϕ = phase separated region, LP = Lifshitz point.

stretching.[15] The transition, analogous to freezing, is from a disordered state (liquid-like) to an ordered state (crystal-like): although the polymer chains locally are amorphous the microstructure has long-range order. The phase diagram shown in Fig. 1, for the PS–PI system, is determined experimentally *via* a combination of SAXS, SANS, TEM and rheology,[16] in comparison with the phase boundary which is predicted theoretically.[17] The phase diagram is presented in terms of the product χN and block copolymer composition, ϕ_I. SCFT predicts spheres (bcc), hexagonally-packed cylinders (hex), cubic *Ia*3*d* (G) and lamellae (lam) which are observed along with the complex hexagonally perforated lamellae (hpl). The most recent experimental studies[18,19] have shown the perforated layer phase to be a long-lived metastable state.

Blending different polymers and yet conserving their individual properties in the final mixture is an extremely attractive and inexpensive way of obtaining new materials with a range of properties that can be precisely tuned by varying the composition of the blend. The entropy of mixing of polymers is generally very low therefore their mixtures generally exhibit a macroscopic phase separation. Only a few systems are reported to be miscible at room temperature and generally show either a lower critical solution temperature and/or an upper critical solution temperature.[20] As a consequence, polymer blends tend to have morphologies that are very dependent on process and thermal history. One way to overcome this natural limitation and increase the compatibility between two dissimilar polymers A/B is to add a compatibilizer to the system such as a block copolymer composed of both A and B species.[2,20] A diblock copolymer, acting as a macromolecular surfactant, segregates at the interface between the two homopolymers, reduces the interfacial tension between the two domains and stabilises microscopic morphologies. Careful control of the composition of such blends can lead to a desirable bicontinuous microemulsion, previously observed in mixtures of water, oil and surfactant,[21] and more recently in ternary blends of two homopolymers and a block copolymer.[22–27] Blends of amphiphilic block copolymers and the corresponding homopolymers as solvents can be considered as model systems where the relative strengths of the interactions can be tuned, in contrast to the oil–water–amphiphile systems that are the subject of many studies, where the peculiar temperature dependence of the hydrophilicity of the surfactant thwarts the comparison of chemically different systems over wide ranges of temperature and composition.[21,25]

Consider the phase diagram of a three component system comprising two immiscible liquids and an amphiphile; these could be oil, water and a surfactant or polymer A, polymer B and an A–B block copolymer. At equal volumes of the immiscible components there is an isopleth shown as the shaded plane in Fig. 2a. At low amphiphile concentrations there are not enough surface active molecules to stabilise the interfaces and phase separation occurs whereas at high amphiphile concentrations a lamellar liquid crystalline phase is formed. At intermediate concentrations of amphiphile, stable microemulsions are formed which are characterised by a high internal surface area. In oil–water–surfactant systems the temperature dependent nature of the amphiphilicity of the surfactant means that the intrinsic surface curvature changes sign. Oil-in-water microemulsions are stable at low temperatures and water-in-oil microemulsions are stable at high temperatures with bicontinuous microemulsions at intermediate temperatures. The amphiphilicity of block copolymers in their parent homopolymers is only very weakly temperature dependent and experimental systems can be designed such that the critical point of the homopolymer blend is the same as the ODT of the block copolymer. The mean-field theoretical calculation[22,28,29] of the phase diagram for a ternary blend of two incompatible homopolymers and the corresponding diblock copolymer shows an isotropic Lifshitz Point, as shown schematically in Fig. 2b. At that point, the two branches of the critical transition meet: a lamellar-disordered ODT line, characterised by a peak at finite q values in a scattering experiment (*i.e.* $q^* \neq 0$) and a two-phase disorder transition line, with $q^* = 0$. Composition fluctuations, however, suppress this Lifshitz point and instead, a bicontinuous microemulsion is experimentally observed around the unbinding transition[22–27] as shown in Fig. 2c. Matsen[30] has recently developed self-consistent field theory that enables the computation of the elastic properties of diblock monolayers in blends of copolymer with two homopolymers.[12] The critical behaviour of symmetric

blends of poly(ethylethylene) and poly(dimethylsiloxane) containing a corresponding symmetric diblock with a higher chain length (the ratio of the degree of polymerisation of the homopolymers and copolymer was $\alpha=(N_{PEE}N_{PDMS})^{1/2}/N_{PEE-PDMS}=0.178$) has recently been investigated in detail *via* small-angle neutron scattering.[24,26] The focus was on the low diblock content region of the phase diagram, near the microemulsion phase. It was shown that with increasing diblock content a crossover occurred from 3-D Ising behaviour to isotropic Lifshitz critical behaviour in the disordered phase. These two regimes result from composition fluctuations near the critical point in polymer blends and diblock copolymers respectively. Composition fluctuations suppress the mean-field regime to higher temperatures in both cases.

Phase diagrams showing the existence of microemulsion for polyolefin–polyolefin,[22,23] polyolefin–polyether[25,27] and polyolefin–polydimethylsiloxane[24,26] blends have been reported, showing that the microemulsion channel can be observed for systems with different molecular weight and chain structure. The purpose of this contribution is the characterisation (by small angle X-ray scattering, transmission electron microscopy and X-ray and neutron reflectivity) of the lamellar and microemulsion phases of ternary blends of homopolymers and block copolymers with particular emphasis on the limits of lamellar stability, the width and location of the microemulsion channel and the distribution of the hompolymers in the block copolymer brush.

Experimental section

Synthesis

Polystyrene, polyisoprene and polystyrene-*block*-polyisoprene were synthesised by anionic polymerisation under high vacuum using glass reactors and break-seals. Styrene (Aldrich) and isoprene (Fluka) were dried over calcium hydride and dibutylmagnesium. Isoprene was further dried over *n*-butyllithium at 0 °C. Cyclohexane, distilled from a polystyryllithium solution, was used as a solvent. The initiator, *sec*-butyllithium (1.3 M in cyclohexane, Aldrich), was used as received. The polymerisations of polystyrene, polyisoprene and polystyrene-*block*-polyisoprene were conducted at 30 °C. The polystyrene-*block*-polybutadiene was obtained from Aldrich and the polybutadiene and deuteropolystyrene were obtained from Polymer Sources Inc. and used as received after suitable characterisation. Molecular weights and polydispersity were determined by GPC using polystyrene standards and a corrective factor of 1.579 was used to calculate the molecular weight of polyisoprene from the equivalent polystyrene value. Copolymer composition was detemined by proton NMR spectroscopy. The polymer characteristics are given in Table 1.

Sample preparation

Blends of PS/PI/PS–PI were prepared by dissolution of the appropriate amounts of polymer in toluene followed by co-precipitation in methanol. 0.2 weight % of 2,6-di-*tert*-butyl-4-methylphenol was added as an antioxidant to prevent their cross-linking. The samples were then allowed to dry under vacuum, at 40 °C, for two weeks. Blends of d-PS/PS–PB were specially prepared for reflectivity experiments from 3% solid solutions in toluene. The films were spun-cast onto optically flat silicon wafers (Compart Technology) using a P-6000 spin coater at either 1500 or 3000 rpm. The samples were subsequently dried to constant mass under vacuum and some were annealed at 140 °C for 2 hours.

Table 1 Molecular characteristics

	M_n/kg mol^{-1} [a]	M_w/M_n [a]	N [b]	r_v [c]	f_{PS} [d]
PS	3.6	1.05	35	35	—
PI	2.2	1.05	32	42	—
PS-PI	14.6	1.02	175	208	0.50
d-PS	8.4	1.05	—	—	—
PB	12.0	1.06	—	—	—
PS-PB	83.6	1.23	—	—	0.36

[a]Determined by GPC. [b]N is the number-average degree of polymerisation. [c]r_v is the overall length of the polymer in segments, normalised to a standard segment volume of 100 cm^3 mol^{-1}. [d]f_{PS} is the volume fraction of polystyrene in the diblock, calculated from ^{1}H NMR.

Small-angle X-ray scattering

Small-angle X-ray scattering (SAXS) experiments were conducted on beamlines at either the synchrotron facility located at the CCLRC Daresbury Laboratory, Warrington, UK, or on beamline DUBBLE, at the European Synchrotron Radiation Facility (ESRF) in Grenoble, France. The X-ray beam was monochromated with Ge (111) crystals and a quartz mirror (Daresbury Laboratories) to wavelengths of 1.54 Å (beamlines 2.1 and 8.2[31]) or 1.41 Å (beamline 16.1), or with a double-crystal monochromator followed by a focusing mirror (beamline DUBBLE[32]), to a wavelength of 1.03 Å. Scattered X-rays were recorded on two-dimensional detectors . Detectors were calibrated for scattering vector using diffraction from a rat tail collagen fibre. Scattering patterns were averaged azimuthally to give the one-dimensional form of intensity (arbitrary units) as a function of the scattering wavevector, $|\mathbf{q}|=q=(4\pi/\lambda)\sin(\theta)$, where 2θ is the scattering angle. Samples were placed in sealed aluminium differential scanning calorimeter (DSC) pans with thin mica windows. The pans were held in a Linkam single-pan DSC cell. Temperature-controlled SAXS experiments were operated at a heating rate of 10 °C min^{-1}, and the SAXS profiles recorded every 6 s. Transition temperatures could be determined with a precision of 1 °C.

Transmission electron microscopy

Prior to microtoming, the samples were annealed for a period of 24 hours in a vacuum oven above the T_g of the PS. A Reichert–Jung ultramicrotome, fitted with a RMC CR-X cryosectionning chamber, was used to obtain ultrathin sections ($\approx$50 to 70 nm) for transmission electron microscopy (TEM). Microtoming was conducted at temperatures from −40 to −60 °C using glass knives. Sections were picked up on 300-mesh copper grids and then exposed in the vapour of a 2% aqueous osmium tetraoxide solution for 1 hour, selectively staining the polyisoprene parts of the material. TEM was done on a Philips CM 10 electron microscope operated at 100 kV.

Cloud point determination

Temperatures of macrophase separation for $\Phi_H>0.93$ ternary blends and for the PS/PI binary blend were determined using two techniques: first visually and then using static light scattering.[33] The cloud point was visually observed as the temperature where the melt aspect changes from clear to turbid. Samples were placed in glass ampoules containing a small magnetic stir bar, degassed and vacuum-sealed to avoid degradation. The blends were heated in a thermostated ($\pm$1 °C) oil bath and stirred until a one-phase, transparent melt solution was obtained. The temperature of the oil bath was then decreased by 1 °C increments and left to equilibrate for twenty minutes. At the temperature of phase separation, the samples became opaque and turbid. In the instrumented static light scattering a beam from a 20 mW He–Ne laser ($\lambda=632.8$ nm) was scattered onto a two-dimensional diffuser. A 512 × 512 pixels CCD camera (SITe 7130-0004, Princeton Instruments) is focused on the diffuser using a fixed focal length lens. The cloud point corresponds to the appearance of the scattering of

the direct beam by the macro-domains. Samples were placed in sealed aluminium DSC pans with thin mica windows. The pans were held in a Linkam single-pan DSC cell and heated to above the temperature of macroscopic phase separation, in the isotropic melt state. The transparent samples were then cooled down at a rate of 1 °C min^{-1}, while the transmitted intensity was recorded every 30 seconds. The intensity detected was plotted as a function of the temperature and the cloud point was identified as the temperature at which the transmitted intensity started to deviate from the baseline by a double tangent construct.

X-Ray reflectivity

Measurements were made at the at the CCLRC Daresbury Laboratory, Warrington, UK on beamline 16.2.[34] The instrument is a diffractometer receiving light inclined at angles of up to 5 degrees from the horizontal. Two primary monochromators equipped with silicon and germanium 111 and 220 crystals provide fixed wavelength of 1.36 Å. The detector used was a solid-state high purity germanium, ten-element detector. The samples are positioned on the stage, where the height alignment was roughly set using a theodolite that had been calibrated to the beam height, then aligned using the beam. The sample is scanned from 0.2 to 2°. The maximum filter attenuation is used at low angle and the attenuation is reduced as the scanning angle increases. A data acquisition protocol was written with differing setups for each overlapping angular range, with successive scans mapped together during the data analysis.

Neutron reflectivity

Measurements were made at the Rutherford Appleton Laboratory on the CRISP instrument.[35] This instrument operates at a fixed geometry, variable λ and detects the wavelength of the incident neutrons *via* a time-of-flight (ToF) set-up. The instrument was fitted with a ^{3}He single detector .The incident beam was set at 1.5°, therefore with a wavelength range of 0.5–6.5 Å, a q-range of 0.05–0.65 $Å^{-1}$ is available. The alignment of the samples with the beam was achieved by changing the height and angle of the sample. A preliminary alignment is performed with a small He–Ne laser which is positioned such that it follows the path of the neutron beam. The sample was then aligned using the neutron beam. The angular range available on this instrument is from 0.2 to 3°. For each sample, a three-stage scan was performed.

Results and discussion

Small-angle X-ray scattering

Temperature-controlled SAXS experiments were performed to identify the lamellar (neat lamellae for the pure polystyrene-*block*-polyisoprene copolymer, and swollen lamellae for $0 < \Phi_H \leqslant 0.77$) and bicontinuous microstructures ($0.79 \leqslant \Phi_H \leqslant 0.93$) and to establish the order–disorder transition temperature.

Lamellae in PS/PI/PS–PI ($0.0 < \Phi_H \leqslant 0.77$). The SAXS profiles of the neat block copolymer typically exhibit a sharp Gaussian peak below the order–disorder transition (ODT) and a broad Lorentzian-like peak above it.[36] The onset of the ODT is characterised by a sudden broadening of the peak accompanied by a sharp drop of the peak intensity (I_{max}), and a shift in the peak position upon heating. The changes in intensity, peak shape and peak position are used to identify the order–disorder transition temperature in diblock copolymers. The protocol for determining the ODT in pure PS–PI diblocks are well known and have been described by Hashimoto *et al.*[37,38] and is used routinely in our laboratory.[36] The SAXS profiles from a ternary blend ($\Phi_H = 0.49$) are shown in Fig. 3

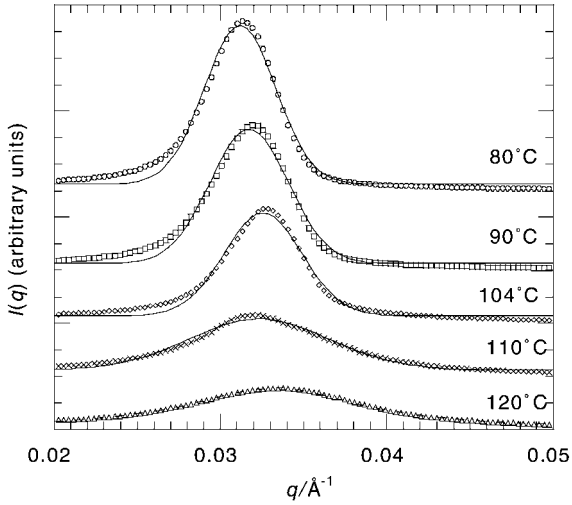

Fig. 3 Temperature dependence of the SAXS profiles for PS/PI/PS–PI $\Phi_H = 0.49$, at selected temperatures around the ODT. The data (symbols) were fitted (lines) using the Gaussian equation (80, 90, 104 and 110 °C) and the Lorentzian equation (120 °C). For clarity, curves have been vertically shifted.

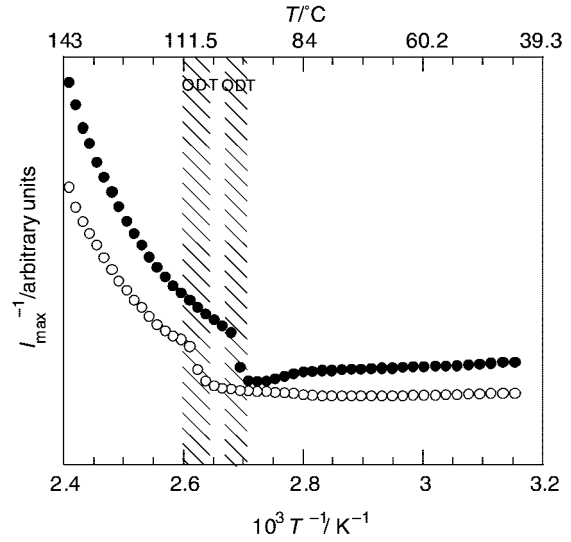

Fig. 4 Temperature dependence of the inverse maximum intensity I_{max}^{-1} (I_{max} is the intensity at q^*) (●) for the neat PS–PI diblock and (○) for a lamellar ternary blend (PS/PI/PS–PI $\Phi_H = 0.49$).

for five temperatures around the ODT, and were taken during a 10 °C min^{-1} temperature ramp. The data are fitted by a Gaussian profile below and a Lorentzian profile above the ODT. All SAXS patterns obtained for lamellae and swollen lamellae are well fitted using either a Gaussian or a Lorentzian equation, yielding the peak position (q^*), the half-width at half-maximum (σ) and the peak intensity at (I_{max}) of diffraction. The periodic spacing (d-spacing, d) of the lamellar phase was calculated from the value of q^* ($d = 2\pi/q^*$). The Gaussian and the Lorentzian fits remain accurate for swollen lamellae, as shown in Fig. 3.

Fig. 4 shows plots of the reciprocal peak intensity ($1/I_{max}$) as a function of the reciprocal temperature ($1/T$) for two different compositions ($\Phi_H = 0.0$ and $\Phi_H = 0.49$). $\Phi_H = 0.49$ is chosen as a representative example for the behaviour of ternary blends exhibiting a swollen lamellar microstructure. The order–disorder transition appears clearly as a sharp increase of $1/I_{max}$ and similar changes are observed in the half-width at half-maximum (σ^2 not shown). The temperature at which these values change discontinuously is the ODT, and is commonly referred to as T_{ODT} revealing a slightly broader ODT for the

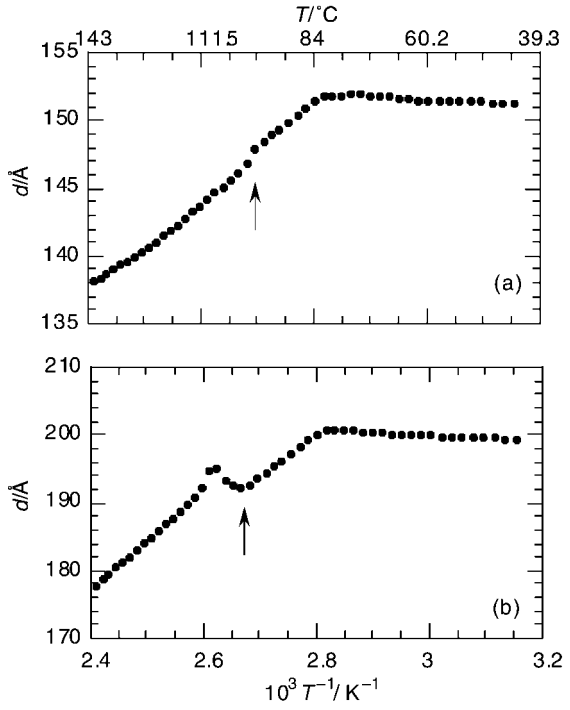

Fig. 5 Temperature dependence of the periodicity d ($d=2\pi/q^*$): (a) for the neat PS–PI diblock and (b) for a lamellar ternary blend (PS/PI/PS–PI $\Phi_H=0.49$). The arrow indicates the ODT.

swollen lamellae, spanning 6 K as compared to the sharp ODT of the pure block copolymer, occurring over less than 4 K at a heating rate of 10 °C min^{-1}, which is confirmed by the behaviour of σ^2 (T). Furthermore, the ODT is shifted to higher temperatures for swollen lamellae compared to the neat block copolymer.

An unusual method accessing T_{ODT} in the ternary blends is a plot of the lamellar d-spacing as a function of reciprocal absolute temperature ($1/T$), as shown in Fig. 5 for $\Phi_H=0.0$ and $\Phi_H=0.49$. Below 84 °C ($1/T=0.0028$ K^{-1}), that is the glass transition of the polystyrene blocks ($T_g^{PS}\sim 80$ °C), d is insensitive to temperature as would be expected for a vitreous system. This is observed for the pure block copolymer, as well as for all the lamellar ternary blends studied. Above the glass transition, d decreases linearly with decreasing $1/T$ (*i.e.*, d decreases with increasing temperature), as anticipated from the temperature dependence of the radius of gyration R_g, of the block copolymer, since $d\propto R_g$. This means that the temperature coefficient of the chain dimensions is of a larger magnitude and opposite in sign to the thermal expansion coefficient of the material. For the pure block copolymer (Fig. 5a), d decreases discontinuously at the ODT. The change we draw attention to is small but worth noting, since it has been previously reported[37–39] that no change in d occurs at the ODT for pure block copolymers. The plot of d *versus* $1/T$ of all ternary blends having $\Phi_H\geqslant 0.29$ (see Fig. 5b for example) shows that d decreases linearly *versus* $1/T$ as expected, however a discontinuous increase of d is clearly visible at the ODT. This behaviour has been reported once before[40] for a symmetric polystyrene-*block*-polyisoprene copolymer, and for polystyrene-*block*-polyisoprene copolymers forming either cylindrical microdomains of polystyrene in a polyisoprene matrix or a bicontinuous microstructure.[38] Furthermore, similar behaviour has been observed in binary mixtures of polystyrene-*block*-polyisoprene copolymers exhibiting cylindrical or bicontinuous microdomains, in contrast with lamellar microdomains exhibiting a continuous increase of d throughout the ODT.[41] Finally, this behaviour has also been observed for a PS–PI diblock copolymer and a PS–PI–PS triblock copolymer

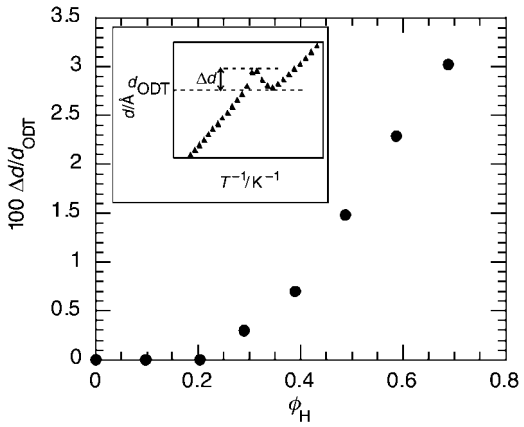

Fig. 6 Composition dependence of the relative thickening, $\Delta d/d_{ODT}$ of the PS/PI/PS–PI lamellae at the order–disorder transition. The inset is a plot of d *versus* T^{-1}, from which Δd is calculated.

reported to self-assemble to micelles in a slightly selective solvent.[43] Ogawa *et al.*[38] interpreted the phenomenon as an effect of chain stretching resulting in an ordering process and the growth of the microdomains. In our ternary system, this behaviour is all the more pronounced as the volume fraction of homopolymers in the blend is increased, as shown in Fig. 6, and finds its justification with the same interpretation: the stretching of the diblock is all the more important at the ODT as the amount of homopolymer is increased, in order to accommodate the extra degree of freedom provided by the homopolymers.

Upon incorporation of homopolymers in the lamellar structure of the pure block copolymer ($d=152$ Å), the microdomains dimensions increase by a factor of 2.5 ($\Phi_H=0.77$; $d=379$ Å) whilst retaining the lamellar structure and without causing macroscopic phase separation. Meanwhile, T_{ODT} increases slightly from 96 °C for the pure diblock to 114 °C for $\Phi_H=0.77$, and the transition gradually broadens. The shape of the diffraction peak, however, remains Gaussian at the ODT up to $\Phi_H=0.77$. Above $\Phi_H=0.79$, the diffraction peak broadens and q^* shifts towards smaller values as Φ_H further increases. From this value ($\Phi_H=0.79$), a Gaussian fit is no longer appropriate to describe the SAXS profiles. The blend characterised by a composition of $\Phi_H=0.79$ appears to exhibit a bicontinuous morphology, as observed both by SAXS and TEM. Some micrographs showed a small fraction of lamellae coexisting with the bicontinuous morphology, however, their proportion is too small to generate a second diffraction peak detectable by SAXS. A region of coexistence between a lamellar and a bicontinuous structure in the phase diagram of a ternary blend of polyethylene oxide–squalane–polyethylene oxide-*block*-polyethylenepropylene ($\Phi=0.17$) has been found at low temperatures by Bates *et al.*[27] In this system, the microemulsion was the only phase present at high temperatures, in blends containing between 9 and 11% of copolymer (mass fraction). As the temperature was decreased an additional diffraction peak appeared, attesting to the presence of a lamellar phase, more stable at lower temperatures relative to the microemulsion. It is important to note that the polyethylene oxide–squalane–polyethylene oxide-*block*-polyethylenepropylene system comprises much lower molecular weight compounds, allowing the structure to equilibrate more rapidly at low temperatures. The coexistence of both lamellar and bicontinuous microstructures in measurable proportions has not been observed by SAXS in our system involving polymers having higher molecular weight.

Bicontinuous microemulsion in PS/PI/PS–PI ($0.79\leqslant\Phi_H\leqslant 0.93$). The diffraction peak exhibited in SAXS moves progressively towards smaller q values with increasing Φ_H. For

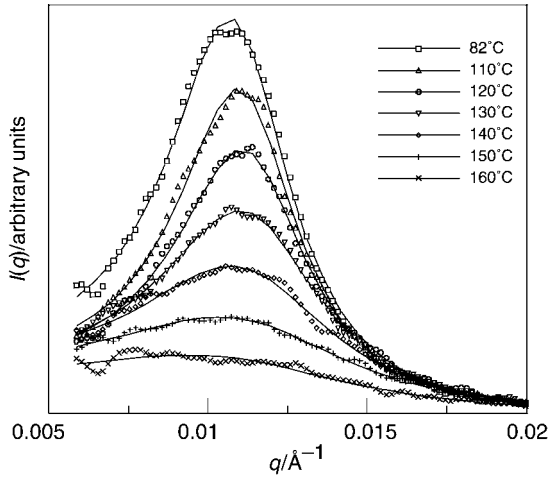

Fig. 7 Temperature dependence of the SAXS profiles for the PS/PI/PS–PI $\Phi_H = 0.86$ blend, at selected temperatures. The data (symbols) were fitted (lines) using the Teubner–Strey equation.

$\Phi_H \geqslant 0.79$, the peak at low temperatures is no longer Gaussian in shape. Teubner and Strey have developed an expression for the scattering by bicontinuous microemulsions:[43]

$$I(q) \sim \frac{1}{a_2 + c_1 q^2 + c_2 q^4} \quad (4)$$

To describe the scattering curves of microemulsions, a_2 should be >0, $c_1 < 0$ and $c_2 > 0$. The negative c_1 tends to create interfaces and the positive c_2 stabilises the system. This function (eqn. 4) presents a maximum with the high q side of the peak decaying as q^{-4}. The Teubner–Strey equation takes into account two length scales: the correlation length ξ and the domain size d (associated with the peak position, q^*).

$$\xi = \left[\frac{1}{2}\left(\frac{a_2}{c_2}\right)^2 + \frac{c_1}{4c_2}\right]^{-1/2} \quad (5)$$

$$d = 2\pi\left[\frac{1}{2}\left(\frac{a_2}{c_2}\right)^{1/2} - \frac{c_1}{4c_2}\right]^{-1/2} \quad (6)$$

The Teubner–Strey equation has been applied here to describe the SAXS scattering curves for $\Phi_H \geqslant 0.79$. Fig. 7 shows the scattered intensity as a function of the scattering vector q for $\Phi_H = 0.86$, at various temperatures close to the transition. The dashed lines are calculated according to the model of Teubner and Strey and describe the experimental data reasonably well. According to Teubner and Strey, in a homogeneous isotropic liquid, $a_2 > 0$, $c_1 > 0$ and c_2 vanishes. Therefore, in our system, one should be able to observe the crossover to the isotropic state in the evolution of those coefficients. Unfortunately, the large dimensions of the microstructure drive the scattering peak to low q values, very close to the beam stop. Above 150 °C, the scattered intensity is very weak, resulting in unreliable SAXS data for fitting. Nevertheless, it appears that the microemulsion is still thermally stable, even 50 degrees above the ODT of the block copolymer.

The plots of ξ and d as a function of temperature T (Fig. 8), for $\Phi_H = 0.86$ contain information about the development of the transition and the persistence of the morphology. ξ remains stable at ~430 Å below 108 °C, and decreases linearly at higher temperatures. At approximately the same temperature, d drops from ~572 to ~552 Å and seems to level off. The change in ξ is indicative of the increase in thermal fluctuations at the interface between the microdomains, as the temperature is increased above 108 °C, reducing the length over which the compositional fluctuations are correlated. This results in a thickening and a softening of the interfaces. The stabilisation of

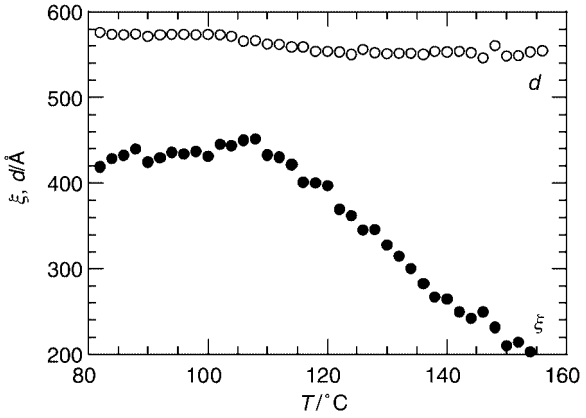

Fig. 8 Length scales d and ξ calculated from the Teubner–Strey model, as a function of temperature, for the PS/PI/PS–PI $\Phi_H = 0.86$ blend.

d suggests that the microemulsion remains stable, even at 152 °C (*i.e.*, 40 degrees above nearest ODT), although it is highly mobile and fluctuating. It is conceivable, and corroborated by mechanical spectroscopy measurements, that the bicontinuous morphology persists even at relatively high temperatures.[44] A plot of $1/I_{max}$ *versus* $1/T$ for the microemulsion has pronounced curvature indicating that mean-field behaviour is not operand, however, because we cannot rely on the diffracted intensity at temperatures above 152 °C, it is not possible to determine whether or not the mean-field isotropic state exists and/or has been attained.

The channel of bicontinuous microemulsion extends for volume fraction of homopolymers up to $\Phi_H = 0.93$. Above this value, the scattering profiles are monotonic functions of q and no diffraction peak is visible, suggesting a macroscopic phase separation involving large length-scales. Scattering profiles recorded for $0.86 < \Phi_H \leqslant 0.93$ blends exhibit a discernible diffraction peak, very close to the beam stop, associated with very large bicontinuous domains. Unfortunately, the limited quality (in terms of counting statistics) of the scattering patterns does not allow a quantitative analysis of the microstructure.

Transmission electron microscopy

The micrographs presented in Fig. 9 confirm the SAXS results and the description of the morphologies. The PS–PI block copolymer presents a lamellar morphology (Fig. 9a), consistent with its composition. As homopolymers are introduced in the respective microdomains, the dimensions increase, as evidenced by the increase of the periodicity as determined by SAXS. This is clearly seen in the micrograph of the $\Phi_H = 0.59$ blend (Fig. 9b), as compared to the micrograph of the pure diblock (the scale is nearly doubled). Fig. 9c shows the microstructure of a $\Phi_H = 0.86$ blend. It is clearly not lamellar anymore but neither is it macrophase separated. The domains are visibly much bigger and the morphology is homogeneous over long distances, yet the bicontinuity of the two interpenetrated networks is not obvious. This may be a consequence of the softness of the sample at room temperature. The thin section (~50–70 nm thick) is neatly cut at −50 °C, but when it warms up back to room temperature for the TEM measurements, the surface becomes rough. This may cause the TEM micrograph to appear blurred. TEM micrographs of phase-separated blends are not presented here since it is very difficult to obtain ultrathin sections of such blends for TEM measurements.

Phase diagram

Using similar SAXS procedures as detailed above for the blends with $\Phi_H = 0.49$ and $\Phi_H = 0.86$, the order–disorder

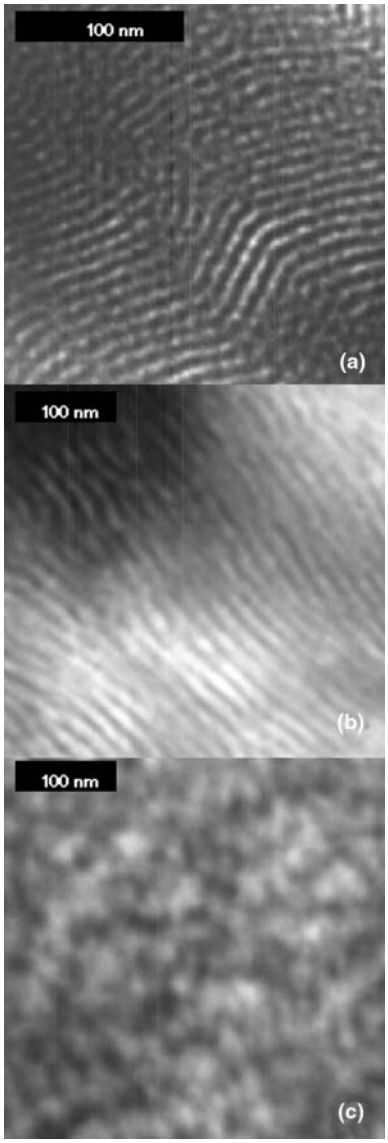

Fig. 9 TEM micrographs (a) for the PS–PI diblock copolymer (lamellar microdomains); (b) for the PS/PI/PS–PI $\Phi_H = 0.49$ blend (swollen lamellar microdomains) and (c) for the PS/PI/PS–PI $\Phi_H = 0.86$ blend (bicontinouous microemulsion).

transition temperatures and the domain microstructures for a number of other blends covering the whole range of compositions going from $\Phi_H = 0$ to $\Phi_H = 1$ have been determined. The boundaries between the high-temperature disordered state and 3 ordered phases have been defined as: periodically ordered phase (lamellar) between $\Phi_H = 0$ and $\Phi_H \approx 0.77$; bicontinuous microemulsion between $\Phi_H \approx 0.79$ and $\Phi_H \approx 0.93$; uniformly ordered (macrophase separated) at $\Phi_H > 0.94$. Fig. 10 gives the experimental phase diagram for the ternary blends investigated in this study, in terms of T_{ODT}, determined by SAXS, and temperatures of macroscopic phase separation ($T_{2\varphi}$). $T_{2\varphi}$ were determined either by cloud point measurements or by static light scattering. However, the phase separated region has not been studied in detail. The positions of the boundaries are remarkably similar to experimental phase diagrams published elsewhere[22–27] and the liquid phase behaviour of ternary A/B/A–B polymer blends (with no specific interactions) are universal. It is of interest to observe in Fig. 10 that the T_{ODT} of the blends displaying a lamellar microstructure are slightly higher than the T_{ODT} of the pure block copolymer and that the T_{ODT} increases monotonically with increasing Φ_H.

Although we have been able to determine by SAXS and

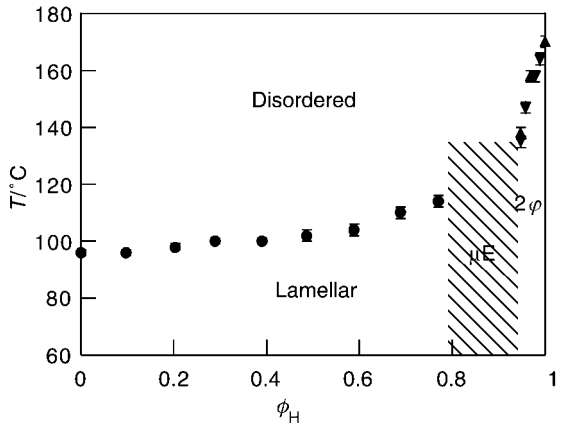

Fig. 10 The Φ_H–T isopleth at $\Phi_S = 0.5$ of the PS/PI/PS–PI phase diagram. The phase boundaries were obtained by a variety of techniques: (●) order–disorder transitions observed by SAXS; (▼) phase separation as determined by cloud point measurements; (▲) phase separation as determined by static light scattering; μE: microemulsion channel; 2φ = phase separated region.

mechanical spectroscopy the approximate temperature at which the transition from the microemulsion to the isotropic melt starts, for 3 compositions ($\Phi_H = 0.79$; 0.82 and 0.86), we have not reported these values on the phase diagram. The presence of such a boundary between the microemulsion and the disordered state is unclear. The ODT of block copolymers has been studied in some detail[2,36–39,44] and is a weakly first-order transition to a non-mean-field disordered state characterised by thermal fluctuations. These fluctuations are subsequently suppressed with increasing temperature and a mean-field behaviour is recovered.[44] The composition fluctuations are manifest in Fig. 4, for a $\Phi_H = 0.49$ ternary blend, causing the initial curvature in the I_{max}^{-1} *versus* T^{-1} plot above the ODT. From our results, it appears that ternary blends exhibiting lamellar morphology behave like typical symmetric diblocks. In contrast, the microemulsion in ternary blends is formed due to the suppression of the Lifshitz point (and unbinding transition) by fluctuations. Thus, the transition from a bicontinuous microemulsion to an isotropic state is expected to be from a fluctuating disordered phase to a fluctuating ordered phase and we have not been able to access the mean-field regime where the thermal fluctuations vanish.

The characteristic length scales of the morphologies as a function of the composition are presented in Fig. 11. It is interesting to observe that upon the incorporation of homopolymers in the lamellar microstructure of the diblock, the periodic spacing can increase up to 2.5 times its original value

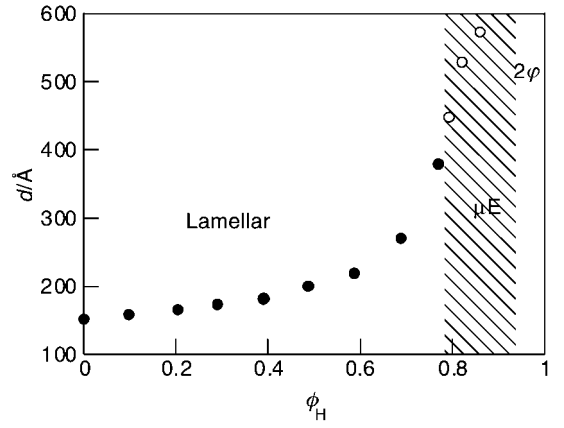

Fig. 11 Composition dependence of the PS/PI/PS–PI characteristic lengths (●) d, periodic spacing in the lamellar structure, below T_g^{PS}; (○) d, periodic spacing in the microemulsion, calculated from the Teubner–Strey model.

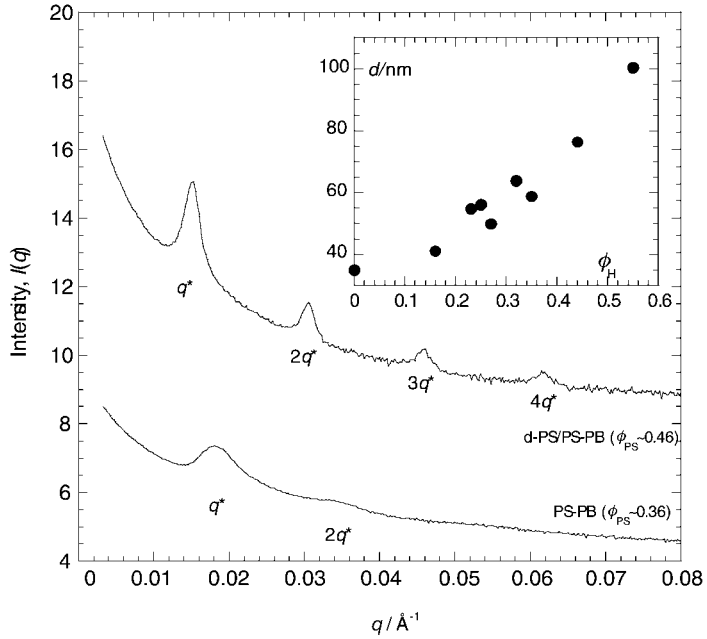

Fig. 12 SAXS profiles for neat block copolymer PS–PB ($\Phi_S = 0.36$) and blend d-PS/PS–PB ($\Phi_S = 0.46$). The inset is the d-spacing *versus* the volume fraction of homopolyer for d-PS/PB/PS–PB with $\Phi_S \sim 0.5$.

($\Phi_H = 0.77$; $d = 379$ Å), without destruction of the microstructure. Further increase of the homopolymer fraction results in the development of the bicontinuous microstructure, characterised by an even larger periodicity varying between 450 Å ($\Phi_H = 0.79$) and 570 Å ($\Phi_H = 0.86$). Considering that the homopolymers are 5 times smaller than the block copolymer ($\Phi = N_H/N_{PS-PI} = 0.19$), the swelling of the lamellar structure and the development of the microemulsion must be accompanied by a large stretching of the diblock chains if the homopolymer is uniformly distributed.

The distribution of homopolymer in PS/PB/PS–PB blends

In order to investigate the distribution of homopolymer in blends of block copolymers an unsymmetrical block copolymer with a larger lamellar spacing than the materials reported earlier was selected for study. The techniques of choice[45–50] are X-ray and neutron reflectivity, which allow determination of in-plane structure, and the block polymer was diluted with deuterated PS and hydrogenous PB, the deuterium labelling providing the majority of the contrast in the neutron reflectivity[48] whereas the electron density differences provide the contrast in the X-ray reflectivity[48] measurements. The block copolymer had a volume fraction of PS $\phi_{PS} = 0.36$ and this allowed dilution with d-PS to make a lamellar system which is used as an example herein. A wide range of homopolymer concentrations (both d-PS and PB) were studied and the overall conclusions are presented here.

Fig. 12 shows the SAXS patterns for a d-PS/PS–PB binary blend ($\phi_S = 0.46$) compared to the neat diblock copolymer. The addition of 20 wt% of d-PS gave a sample with a well-defined lamellar morphology as shown by the sharp Bragg peaks and the regular spacing between the reflections. It was also observed that the first-order peak had shifted to lower q upon addition of homopolymer and that the long-range order in the system was improved compared to the neat block copolymer. This suggested that the lamellae had swollen, resulting in larger d-spacing, as previously reported[51,52] for similar blends and as anticipated by the results reported in Section 3.1. A wide range of compositions were studied and the relationship between the volume fraction of homopolymer and the d-spacing is given as an inset to Fig. 12 which can be compared with the data for PS/PI/PS–PI in Fig. 11.

X-Ray reflectivity was used to investigate the morphology of spun cast films, and yielded information on the internal structure and the total film thickness.[48] The X-ray contrast results from the difference in electron density within the samples. The block copolymers studied here contain only hydrogen and carbon, resulting in poor contrast and only limited information on the internal morphology of the films was extracted. However, X-ray reflectivity is an ideal tool to investigate the total film thickness as there is sufficient contrast between air, the film and the Si substrate to obtain reflections from the air–film and the film–substrate interfaces and this information is used in modelling the structure from neutron reflectivity.

The isotopic dependence of neutron scattering length densities allows specific labelling compared to electron densities. The large scattering length density of d-PS introduces a large contrast into the system. Fig. 13 shows a neutron reflectivity curve with the associated error bars. The sample is a

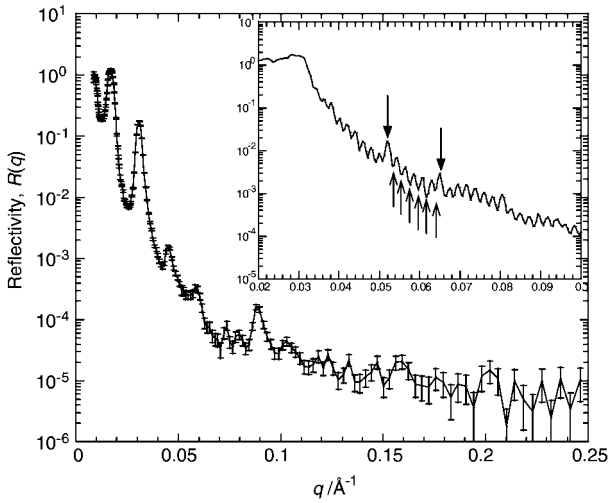

Fig. 13 Neutron reflectivity profile for an as-prepared film of d-PS/PS–PB ($\Phi_S = 0.46$). The reflectivity is dominated by Bragg peaks from the internal film structure at low q. The inset is the X-ray reflectivity from the same sample with the Kiessig fringes from the total film thickness marked with up-arrows and the Bragg peaks from the internal structure marked with down-arrows.

d-PS/PS–PB blend with $\phi_{PS}=0.46$ spun-cast at 1500 rpm. The errors at low q are rather small, but increase with increasing q becoming noisy above $q=0.1$ Å^{-1}. The neutron reflectivity profile is dominated by Bragg diffraction from the lamellae. The first order peak is at $q=0.015$ Å^{-1}, and peaks up to the sixth order can be observed. The lamellar spacing is the same as that observed in the bulk SAXS (at $q=0.015$ Å^{-1}) and the random-grain lamellar morphology from the bulk sample has been transformed into an oriented lamellar morphology in spun-cast films. The X-ray reflectivity curve for the same sample is given as an inset, the curve is dominated by a high frequency oscillation from the total film thickness and the minima from these Kiessig fringes are indicated by up-arrows. The spacing between the minima can be used to estimate the total film thickness that in this case is 300 nm corresponding to approximately 7 lamellar repeats of 42 nm. Furthermore there

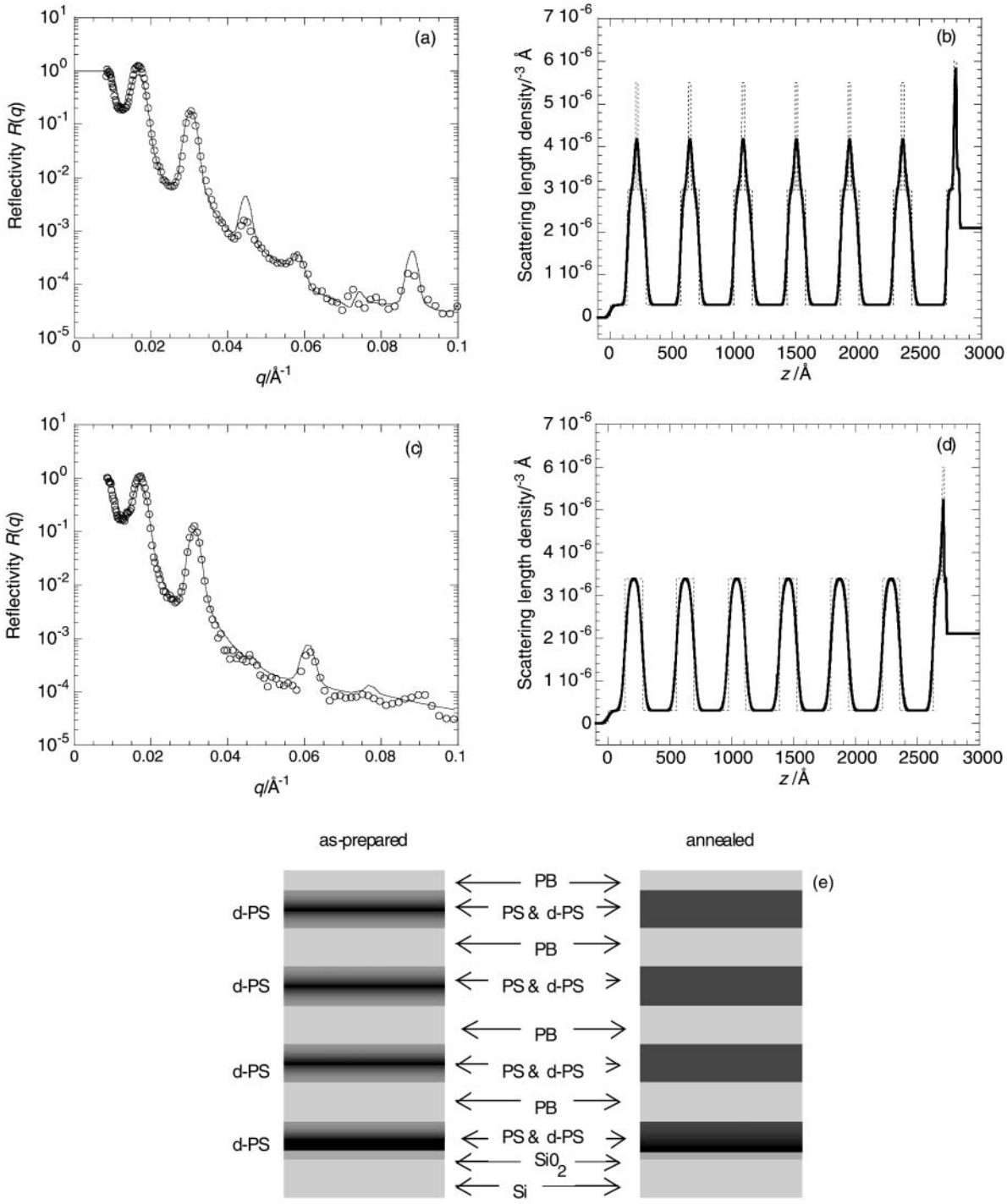

Fig. 14 (a) Neutron reflectivity for d-PS/PS–PB ($\Phi_S=0.46$) (a) experimental (○) and fitted (—) reflectivity for the film spun-cast at 1500 rpm. (b) The initial slab model (dotted line) and the refined scattering length density profile (thick line) for reflectivity fitted in (a). (c) Experimental (○) and calculated (—) reflectivity for the film spun-cast at 1500 rpm and subsequently annealed. (d) The initial slab model (dotted line) and the refined scattering length density profile (thick line) for reflectivity fitted in (c). (e) A schematic of the film structure with the density of greyscale indicating the scattering length density. In both the annealed and as-prepared samples d-PS is preferentially adsorbed at the polymer–SiO_2 interface where there is a half thickness layer and at the air–polymer interface there is a half layer of PB. The d-PS is segregated in the middle of the PS layers after spin casting and on annealing for 2 hours above the T_g of polystyrene becomes uniformly distributed.

are also Bragg peaks in the X-ray reflectivity (marked by down-arrows) and these have a Δq of 0.015 $Å^{-1}$ confirming that the sample comprises oriented lamellar morphology.

Neutron and X-ray reflectivity experiments have also been used to investigate the effect of film processing on the internal film morphology, and on the total film thickness. The effect of increasing the spin-speed was to make thinner films as expected, however the processing had no effect on the internal layer thickness and the average d-spacing was a constant. Previous studies of spun-cast block copolymers indicate that annealing is an important factor in obtaining representative structures[45] but, as can be seen from the data in Fig. 14a and 14c, annealing has no effect on the position of the peaks and the overall lamellar thickness but, due to some reorganisation of the labelled polymer, can be responsible for the loss of higher order reflections. The films were subjected to annealing in order to improve the ordering of the lamellae within the samples. Previous studies have observed that annealing allowed the polymer chains to relax, and for a lamellar system, this resulted in well-defined interfaces.[53] The effect of annealing observed in this work suggested that either the surface or the lamellae interfaces had their roughness increased. Diffuse reflection is induced by roughness, and this could lead to a reflectivity curve with a missing reflection peak or a reduced intensity.

To extract more information from the reflectivity profiles of the as-prepared and annealed films a computer model of the structure was developed that could be refined against the experimental data. The Parratt32 software used for the modelling of neutron reflectivity has been described in detail elsewhere.[54] An initial model of the expected structure of the films must be estimated which can then be refined against the data. The individual layer thicknesses are estimated from the d-spacing and composition of the sample and the total film thickness is obtained from X-ray reflectivity. The scattering length densities are calculated from stoichiometry and measured densities with atomic cross-sections taken from literature and are 6.69, 1.68 and 0.45×10^{-6} $Å^{-2}$ for d-PS, PS and PB respectively.[55] Neutron scattering measurements rely on samples high in neutron contrast, and for copolymers it is often introduced by deuterium labelling one of the blocks. In the present work, the labelling was introduced with a deuterated homopolymer in order to probe the localisation of this polymer in the layers. The location of the deuterated homopolymer was an important parameter in the initial model structure as it affected enormously the goodness of fit and subsequent refinement.

Figs. 14b and 14d present the scattering length density profiles obtained from constrained fits to the reflectivity data in Figs. 14a and 14c. The square wave is a slab construction informed by the lamellar spacing and the bare scattering length densities and is effectively the starting point for structure refinement. The smooth lines in the model are the density profiles that give the best fit to the data and correspond to the slab models with approximately 20 Å root mean squared roughness. An important check on the validity of the model is the sum of the of scattering length densities which is 8.80×10^{-6} $Å^{-2}$ for the experimental data in Fig. 14a compared with 8.83×10^{-6} $Å^{-2}$ for the model in Fig. 14b. Fig. 14e is a schematic of the film structure with the density of greyscale indicating the scattering length density. In both the annealed and as-prepared samples d-PS is preferentially adsorbed at the polymer–SiO_2 interface where there is a half thickness layer and at the air–polymer interface there is a half layer of PB. The d-PS is segregated in the middle of the PS layers after spin casting and on annealing for 2 hours above the T_g of polystyrene becomes uniformly distributed.

The formation of coherent block copolymer films with integer (or integer plus a half) numbers of lamellar stacks is consistent with previous studies[45–50,56,57] on block copolymers. The neutron reflectivity shows a half layer of PS at the lower surface and a half layer of PB at the upper surface and we therefore expect layer thickness with an integral number of lamellar repeats. The spin-casting speed affects the total number of layers, with for example, 7 lamellar repeats at 1500 rpm and 5 lamellar repeats at 3000 rpm. The formation of a segregated structure, with the deuterated homopolymer at the silica–polymer interface is anticipated by previous studies of deuterated/hydrogenous polymer blends[58] where the surface energy difference between the labeled and unlabelled materials is sufficient to provide surface enrichment. This effect is also enhanced by the d-PS having a much lower molecular weight than the PS block in the PS–PB block copolymer. The enrichment of the d-PS homopolymer at the center of the PS layers is also anticipated by previous work on the distribution of homopolymers in block copolymers[59] and SCFT predictions[30] also anticipate formation of dry-brush morphologies in some circumstances. On annealing the d-PS becomes evenly distributed in the layer and the block copolymer structure becomes that of a wet brush.[51,59] It is somewhat surprising that this transition is not associated with a change in the layer thickness but this is obviously not the case as can be observed in the data.

Concluding remarks

In this paper we have determined the ODT, the microdomain structures and the phase diagram for ternary blends of low molecular weight PS, PI and PS–PI and determined the distribution of the homopolymer within the layers of a related PS/PB/PS–PB system. The T_{ODT} and the microstructures, confirmed by TEM, were determined by SAXS and supported by additional mechanical spectroscopy measurements. The SAXS profile of lamellar microstructures of ternary blends did not differ from the ones exhibited by pure symmetric diblocks. It consisted of a Gaussian-like diffraction peak below the ODT, and a Lorentzian-like peak above it, even though the swelling resulted in a periodicity up to 2.5 times bigger than its original value for the neat diblock. The bicontinuous morphology scattering patterns were interpreted in terms of the Teubner–Strey equation, yielding values of the periodic spacing, d, and the correlation length, ξ, of the structure. The position of the microemulsion window, between $\Phi_H \approx 0.79$ and $\Phi_H \approx 0.93$ is predictable using a self-consistent mean-field theory.[30]

The weakly first-order phase transition for the lamellar microstructures (either the neat diblock lamellae or the swollen lamellae of the ternary blends) as well as the onset of the phase transition of the bicontinuous microemulsion have both been detected by SAXS and we observed an increase in the periodicity around the ODT in swollen lamellae, related to chain stretching. Reflectivity measurements on isotopically labelled samples show that the equilibrium structure is a wet brush when the molecular weight of the homopolymers is much lower than that of the block copolymers. The fluctuation-induced bicontinuous microemulsion persists over a large range of temperatures above the beginning of the ODT, even though it is subjected to thermal fluctuations of large amplitude. The temperature stability of the microemulsion is not very well defined. There is no evidence of a crossover from the non-mean-field, highly fluctuating state (where the microemulsion persists), to a mean-field, disordered state in the temperature range we could access.

Acknowledgements

This work was supported by the Engineering and Physical Sciences Research Council (EPSRC) (Grant GR/M22116) which included beamtime at the Daresbury SRS and ISIS. The

X-ray scattering software was provided by the Collaborative Computing Project 13 (CCP13), the Parratt32 neutron reflectivity software was provided by the Han Mietner Institute and tutorial support came from John Howse. The authors gratefully acknowledge the support of beamline scientists Nick Terrill, Graham Clark and Anthony Gleeson at Daresbury, Wim Bras and Igor Dolbnya at the ESRF and Sean Langdridge at ISIS.

References

1 P. Ball, *The self-made tapestry*, Oxford University Press, Oxford, 1998.
2 I. W. Hamley, *The Physics of Block Copolymers*, Oxford University Press, Oxford, 1998.
3 J. M. Seddon, *Biochim. Biophys. Acta*, 1990, **1031**, 1.
4 F. S. Bates and G. H. Fredrickson, *Ann. Rev. Mater. Sci.*, 1996, **26**, 501.
5 E. L. Thomas and R. L. Lascanec, *Philos. Trans. R. Soc. London A*, 1994, **348**, 149.
6 S. Förster, A. K. Khandpur, J. Zhoa, F. S. Bates, I. W. Hamley, A. J. Ryan and W. Bras, *Macromolecules*, 1994, **27**, 6922.
7 E. L. Thomas, D. M. Anderson, C. S. Henkee and D. Hoffman, *Nature*, 1988, **334**, 598.
8 D. A. Hajduk, M. B. Kossuth, M. A. Hillmyer and F. S. Bates, *J. Phys. Chem. B*, 1998, **102**, 4269.
9 K. J. Hanley, T. P. Lodge and C. I. Huang, *Macromolecules*, 2000, **33**, 5918.
10 M. Clerc, P. Laggner, A.-M. Levelut and G. Rapp, *J. Phys. II*, 1995, **5**, 901.
11 V. Luzzatti, *Nature*, 1968, **218**, 1031.
12 F. S. Bates, M. F. Schultz, A. K. Khandpur, S. Förster and J. H. Rosedale, *Faraday Discuss.*, 1995, **98**, 7.
13 I. W. Hamley, S. M. Mai, A. J. Ryan, J. P. A. Fairclough and C. Booth, *Phys. Chem. Chem. Phys.*, 2001, **3**, 2972.
14 M. W. Matsen and F. S. Bates, *Macromolecules*, 1996, **29**, 1091.
15 M. W. Matsen and F. S. Bates, *Macromolecules*, 1996, **29**, 7641.
16 A. K. Khandpur, S. Förster, F. S. Bates, I. W. Hamley, A. J. Ryan, W. Bras, K. Almdal and K. Mortensen, *Macromolecules*, 1995, **28**, 8796.
17 L. Leibler, *Macromolecules*, 1980, **13**, 1602.
18 M. E. Vigild, K. Almdal, K. Mortensen, I. W. Hamley, J. P. A. Fairclough and A. J. Ryan, *Macromolecules*, 1998, **31**, 5702.
19 D. A. Hajduk, H. Takenouchi, M. A. Hillmyer, F. S. Bates, M. E. Vigild and K. Almdal, *Macromolecules*, 1997, **30**, 3788.
20 G. C. Eastmond, *Adv. Polym. Sci.*, 1999, **149**, 59.
21 M. Kahlweit, *Science*, 1988, **240**, 617.
22 F. S. Bates, W. W. Maurer, T. P. Lodge, M. F. Schulz, M. W. Matsen, K. Almdal and K. Mortensen, *Phys. Rev. Lett.*, 1995, **75**, 4429.
23 F. S. Bates, W. W. Maurer, M. P. Lipic, M. A. Hillmeyer, K. Almdal, K. Mortensen, G. H. Fredrickson and T. P. Lodge, *Phys. Rev. Lett.*, 1997, **79**, 849.
24 D. Schwahn, K. Mortensen, H. Frielinghaus and K. Almdal, *Phys. Rev. Lett.*, 1997, **82**, 5056.
25 M. A. Hillmeyer, W. W. Maurer, T. P. Lodge, F. S. Bates and K. Almdal, *J. Phys. Chem. B*, 1999, **103**, 4814.
26 D. Schwahn, K. Mortensen, H. Frielinghaus, K. Almdal and L. J. Kielhorn, *Chem. Phys.*, 2000, **112**, 5454.
27 N. R. Washburn, T. P. Lodge and F. S. Bates, *J. Phys. Chem. B*, 2000, **104**, 6987.
28 D. Broseta and G. H. Fredrickson, *J. Chem. Phys.*, 1990, **93**, 2927.
29 R. Holyst and M. J. Schick, *Chem. Phys.*, 1992, **96**, 7728.
30 M. W. Matsen, *J. Chem. Phys.*, 1999, **110**, 4658.
31 W. Bras, G. E. Derbyshire, A. J. Ryan, G. R. Mant, A. Felton, R. A. Lewis, C. J. Hall and N. J. Greaves, *Nucl. Instrum. Methods Phys. Res.*, 1993, **A329**, 587.
32 W. Bras, *Macromol. Sci., Phys.*, 1998, **B37**, 557; http://www.esrf.fr/exp_facilities/BM26/BM26.html
33 Y. Ishii and A. Ryan, *J. Macromolecules*, 2000, **33**, 158.
34 http://www.srs.dl.ac.uk/ncd
35 J. Penfold, *Prog. Colloid Polym. Sci.*, 1990, **81**, 198; http://www.srs.isis.rl.ac.uk/largescale/crisp/documents/neut_refl_HD
36 S. M. Mai, J. P. A. Fairclough, I. W. Hamley, M. W. Matsen, R. C. Denny, B. X. Liao, C. Booth and A. J. Ryan, *Macromolecules*, 1996, **29**, 6212.
37 N. Sakamoto and T. Hashimoto, *Macromolecules*, 1995, **28**, 6825.
38 T. Ogawa, N. Sakamoto, T. Hashimoto, C. D. Han and D. M. Baek, *Macromolecules*, 1996, **29**, 2113.
39 F. S. Bates, J. H. Rosedale and G. H. Fredrickson, *J. Chem. Phys.*, 1990, **92**, 6255.
40 B. Stuhn, R. Mutter and T. Albretch, *Europhys. Lett.*, 1992, **18**, 427.
41 D. Yamagushi, T. Hashimoto, C. D. Han, D. M. Baek, J. K. Kim and A. C. Shi, *Macromolecules*, 1997, **30**, 5832.
42 T. P. Lodge, X. Xu, C. Y. Ryu, I. W. Hamley, J. P. A. Fairclough, A. J. Ryan and J. S. Pedersen, *Macromolecules*, 1996, **29**, 5955.
43 M. Teubner and R. J. Strey, *Chem. Phys.*, 1987, **87**, 3195.
44 J. P. A. Fairclough, A. J. Ryan, S. C. Turner, I. W. Hamley, S. M. Mai, C. Booth and R. C. Denny, *Phys. Chem. Chem. Phys.*, 1999, **1**, 2093.
45 A. M. Mayes, T. P. Russell, S. K. Sajita and C. F. Majkrzak, *Macromolecules*, 1992, **25**, 6523.
46 S. P. Gido, J. Gunther, E. L. Thomas and D. Hoffman, *Macromolecules*, 1993, **26**, 6523.
47 T. P. Russell, A. Menelle, S. H. Anastasiadis, S. K. Sajita and C. F. Majkrzak, *Macromolecules*, 1991, **24**, 6263.
48 W. H. de Jeu, P. Lamboy, I. W. Hamley, D. Vankin, J. S. Pedersen, K. Kjaer, R. Seyger, P. van Hutton and G. Hadziiannou, *J. Phys. II*, 1993, **3**, 139.
49 S. H. Anastasiadis, T. P. Russell, S. K. Sajita and C. F. Majkrzak, *J. Chem. Phys.*, 1990, **92**, 5677.
50 N. Koneripalli, R. Levicky, F. S. Bates, M. W. Matsen, S. K. Sajita, J. Anker and H. Kaiser, *Macromolecules*, 1998, **31**, 3498.
51 S. Kiozumi, H. Hasegawa and T. Hashimoto, *Macromolecules*, 1994, **27**, 6532 and 7893.
52 K. I. Winey, E. L. Thomas and L. J. Fetters, *Macromolecules*, 1992, **25**, 2645.
53 R. J. Albalak, E. L. Thomas and M. S. Capel, *Polymer*, 1997, **38**, 3819.
54 L. G. Parratt, *Phys. Rev.*, 1954, **95**, 359; http://www.hmi.de/bensc/software/refl/parratt
55 C. L. O. Salou, PhD Thesis, University of Sheffield, 2000.
56 B. Collin, D. Chatenay, G. Coulon, D. Ausserre and Y. Gallot, *Macromolecules*, 1992, **25**, 1621.
57 G. Coulon, B. Collin, D. Ausserre, D. Chatenay and T. P. Russell, *J. Phys.*, 1990, **51**, 2801.
58 F. S. Bates and G. D. Wignall, *Macromolecules*, 1986, **19**, 932.
59 H. Hasegawa and T. Hashimoto, in *Comprehensive Polymer Science, 2nd Supplement*, ed. S. L. Aggarwal and S. Russo, Pergamon, Oxford, 1996, Ch. 6.